Optics Communications 281 (2008) 4424–4431

Contents lists available at ScienceDirect

Optics Communications

journal homepage: www.elsevier.com/locate/optcom

Speckle characteristics of a broad-area VCSEL in the incoherent emission regime

Falko Riechert [a,*], Guy Verschaffelt [b], Michael Peeters [b,1], Georg Bastian [c], Uli Lemmer [a], Ingo Fischer [b,2]

[a] Light Technology Institute, Universität Karlsruhe (TH), Engesser Str. 13, D-76131 Karlsruhe, Germany
[b] Department of Applied Physics and Photonics, Vrije Universiteit Brussel, Pleinlaan 2, B-1050 Brussels, Belgium
[c] Faculty of Engineering, University of Applied Sciences Trier, Postfach 1826, D-54208 Trier, Germany

ARTICLE INFO

Article history:
Received 6 February 2008
Received in revised form 30 April 2008
Accepted 1 May 2008

OCIS:
(250.7260)
(030.6140)
(110.6150)
(030.1640)
(030.1670)

ABSTRACT

We present a technique to reduce the speckle contrast of a NIR broad-area VCSEL based on the spatially incoherent emission regime that can be obtained when using the proper driving conditions. We evaluate the efficiency of this technique to reduce the speckle contrast by comparing it with the speckle characteristics in multimode emission under cw operation. Depending on the illumination setup, the incoherent emission regime can lead to a strongly reduced speckle contrast down to 1.3%. This is in agreement with estimates of the expected speckle contrast reduction when three contrast reducing effects are taken into account. These low contrast values make the investigated sources attractive for several applications that suffer from speckle noise.

1. Introduction

Since the early 1960s it is known that the illumination of optically rough objects with partially or fully coherent light results in the emergence of a phenomenon currently called speckle [1,2]. Speckle emergence can be justified by stating that each single point of the illuminated surface acts as a secondary source. The phase distribution of all the resulting spherical waves is determined by the random height profile of the surface, leading to a random interference pattern which is called "speckle pattern". Speckle is usually quantified using the contrast C of this interference pattern. The contrast C of a speckle image is the ratio of the standard deviation and the mean value of the intensity levels. A so-called fully developed and fully polarized speckle pattern has a contrast and therefore also a signal-to-noise ratio S/N of 1 [3].

In several applications the emergence of speckle is desirable and useful, e.g. in optical metrology with speckle. Other applications using laser light suffer from speckle because they produce highly degraded images with large intensity fluctuations. This is the case in for example laser projection applications, laser Doppler applications [4] or laser triangulation [5]. For these applications speckle contrast reduction is desirable and essential. A human observer's ability to detect intensity variations on an image has been extensively investigated and is shown to be dependent upon several parameters, including the age of the observer [6], the luminance level [7], the observed colour [8,9] and the temporal and spatial frequency of the fluctuations [10]. Following Wang et al. in [11] a human observer will sense speckle with a contrast larger than about 4%. It is a major challenge to achieve low contrast values in applications using laser light sources. Therefore, one usually combines different speckle reduction techniques. Speckle contrast reduction can be achieved by the intensity-based superposition of several speckle patterns [3]. The minimum achievable speckle contrast $C_{\min.}$ of the superposition of M fully uncorrelated speckle patterns is given by $C_{\min} = 1/\sqrt{M}$. Uncorrelated speckle patterns can be achieved e.g. by reducing the spatial coherence of the illumination source. If the mutually incoherent emission regions of the source's aperture illuminate sufficiently uncorrelated regions on a surface, partially or fully uncorrelated speckle patterns will result. The reduction in spatial coherence of a fully coherent laser source is often obtained by moving or rotating diffusers inserted into the beam path. The beam passes through or is reflected on the surface of a diffuser, which leads to spatial phase scrambling. This solution is not favourable in some applications because it includes mechanically moving parts (diffuser) and the beam shape and quality are degraded. A more preferential method is the use of a laser source, which does not emit fully spatially coherent light. This can be achieved with a laser under cw driving conditions if multiple transverse modes are excited in the cavity.

Even more promising is the recent finding that vertical-cavity surface-emitting lasers (VCSELs) can be driven into a regime of

* Corresponding author. Tel.: +49 7216088756.
E-mail address: Falko.Riechert@lti.uni-karlsruhe.de (F. Riechert).
[1] Present address: Alcatel-Lucent, Copernicuslaan 50, B-2018 Antwerpen, Belgium.
[2] Present address: Joint Research Institute of Integrated Systems and School of Engineering and Physical Sciences, Heriot-Watt University, Edinburgh EH14 4AS, UK.

0030-4018/$ - see front matter © 2008 Elsevier B.V. All rights reserved.
doi:10.1016/j.optcom.2008.05.004

spatially incoherent emission [12]. VCSELs are standard semiconductor laser sources that emit perpendicular to the growth direction of the cavity. Because of the short cavity length of the order of one wavelength, only one longitudinal mode can be lasing. Single-transverse mode operation is achievable with apertures of about 5 μm. For broader apertures and higher cw driving currents the emission of the VCSEL typically consists of a large number of transverse modes. Besides emission in multiple transverse modes, recent investigations of a pulsed broad-area VCSEL have shown that such devices can behave as quasi-homogeneous Shell model sources with reduced spatial coherence [12] when driven by microsecond pulses. The device then no longer shows modal emission. In [12] we attributed this effect to the interplay between the thermal chirp and the build-up of a spatially distributed thermal lens. This leads to the break-up of the global cavity modes. The farfield of the total beam is Gaussian shaped with a full opening angle of 22° [12]. The VCSEL's aperture can then be modelled as being filled with mutually independent Gaussian beamlets each having a coherence radius of approximately 1.4 μm. This value has been calculated from the farfield divergence angle of the VCSEL [12]. It has been independently confirmed by nearfield measurements. Experiments at different pulse amplitudes and lengths have shown that the farfield divergence angle (and thus also the nearfield coherence radius) is only weakly dependent on the pulse parameters once the pulse amplitude and length are large enough to establish the incoherent emission regime. Such a source shows the benefits of a laser source (e.g. the emission of several 100 mW peak output power) while having a Gaussian farfield (opposed to the multi-lobed farfield in modal emission) together with a low degree of spatial coherence (which can be favourable regarding speckle contrast reduction).

In this paper we study the efficiency of the incoherent emission regime in reducing the speckle contrast. Such a complementary technique to reduce speckle is worthwhile investigating, as speckle is a problem not easily solved in many applications. To get a fair idea of the efficiency of this new technique, we compare the speckle reduction in the incoherent emission regime and under cw multimode operation.

The remainder of the paper is organized as follows. In Section 2 we will describe the experimental setup. In Section 3 we show the speckle contrast measurements when our broad-area VCSEL is driven in different regimes in different setups. Section 4 deals with the different effects that influence the obtained speckle contrast. In Section 5 we will estimate the speckle contrast for the various illumination setups and driving conditions to then compare the estimates with the experimental findings. In Section 6 we try to draw conclusions concerning how the spatially incoherent emission from broad-area VCSELs can effectively be used to reduce the speckle contrast.

2. Setup and principles of speckle measurements

We use a native oxide confined VCSEL, which emits light at an approximate wavelength of 850 nm and has an aperture diameter of 50 μm. The characterization and detailed parameters of the device can be found in [12]. The VCSEL is mounted on a heat sink to stabilise the mount temperature to room temperature. For cw operation we use a current source with an accuracy of +/− 0.1% of the driving current. In case of pulsed operation of the VCSEL, an arbitrary waveform generator with a 50 Ω output impedance and a 50 MHz bandwidth is used.

The CCD-camera used in the speckle measurements is a 12-bit linear camera (TechnoTeam, type LMK 98-3) with variable integration time. It is used with a "Tamron TT18" objective which has a focal length of 18 mm and a working distance of 9.7 cm. In focus, the full field of view corresponds to about 1 cm^2. The camera supports automatic correction of systematic errors, e.g. an edge decay of the optical elements. We performed all measurements in reflection from a paper screen (standard 80 g/m^2 office paper, manufacturer: Storaenso, type: berga speed).

Measurements of absolute speckle contrast values have to be performed carefully for several reasons. Any movement in the measurement setup has to be suppressed. The camera taking the speckle picture has a given integration time (typically several microseconds). If the illuminated screen or the camera is moved during the integration time, the speckle image on the CCD chip changes. This leads to unwanted smearing of the speckle image on the CCD and therefore to a lower speckle contrast. Furthermore, the size of the spots in the speckle pattern has to be sufficiently large. One spot in the speckle pattern has to be larger than approximately ten CCD pixels for proper contrast measurement. A speckle image shows an exponentially decaying probability density function of the measured intensity values [3]. Therefore ambient light has to be reduced as much as possible. We took images – the VCSEL being switched off – with different integration times of the camera to determine the background intensity values caused by camera noise and ambient light. The background intensity was typically between 0.1% and 0.5% of the mean intensity measured in the experiments (see Section 3) when the VCSEL is switched on. This is sufficiently small to be neglected. The accuracy with which the speckle contrast can be determined is mainly restricted by the (large scale) homogeneity of the captured images. To minimize errors in the determination of the speckle contrast, diverse regions of interest are taken into account in order to determine a medium speckle contrast.

To check the stability of the setup and to show that there is no relevant influence of camera noise and ambient light, we first performed measurements with an argon ion laser emitting approximately 3.5 mW into a polarized TEM_{00} beam. The laser was mounted at a distance of 1 m from the screen and illuminated the screen directly with only a small angular offset. The camera was placed in the farfield of the screen at a distance of 1.2 m (again with only a small angular offset). We measured a speckle contrast of 70.8% which is in excellent agreement with the theoretical value (see Section 4.1) of $1/\sqrt{2}$ that we expect for our fully depolarizing paper screen when illuminated by a fully coherent monochromatic source.

3. Measurements

3.1. Driving conditions

We operate the VCSEL under different cw and pulsed driving conditions summarized in Table 1. In cw operation, we drove the VCSEL with three different currents: 20 mA (just above the threshold current), 60 mA (halfway to the maximum driving current) and

Table 1
Driving parameters of the VCSEL in cw and pulsed operation

Cw operating conditions	
Driving current	
20 mA (just above threshold)	
60 mA (intermediate)	
100 mA (nearby maximum)	
Pulsed operating conditions	
Pulse lengths	Pulse height
100 ns, 1000 ns and 2000 ns	32 mA
100 ns, 1000 ns and 2000 ns	124 mA
100 ns, 1000 ns and 2000 ns	274 mA

100 mA (close to the thermal roll-over point of the VCSEL's PI characteristic). In pulsed operation, three pulse heights and durations were investigated. Using a pulse with an amplitude of 32 mA, the VCSEL emits in multiple transverse modes irrespective of the pulse duration. For pulses with larger amplitude (124 mA and 274 mA), the emission depends on the pulse duration [12]. For a pulse length of 100 ns, which is much shorter than the thermal time-scale of the VCSEL, we still observe modal emission. When the pulse length is increased to 1 μs and 2 μs (while keeping the amplitude at 124 mA or 274 mA), the VCSEL emits a spatially incoherent beam. We limit the maximum pulse length to 2 μs as this is the longest pulse duration which can be used before modal effects reappear in the VCSEL emission. For all of the pulsed driving conditions, the duty cycle is set to 1% to avoid any average heating of the VCSEL.

3.2. Measurement setups

In Figs. 1–4a we show the different setups used to characterize the speckle behaviour of the VCSEL. We either project the nearfield of the VCSEL via a doublet lens onto the screen (Figs. 1 and 2a) or we directly shine the farfield of the VCSEL onto the screen (Figs. 3 and 4a). Also for the CCD-camera we use two different positions. The camera is either imaging the screen (Figs. 1 and 3a) or the camera is placed in the farfield of the screen (Figs. 2 and 4a). In case of the nonmodal emission, the VCSEL's beam only has to propagate further than 20 μm before the farfield regime is entered [12,13]. In case of modal emission, the farfield regime is reached at a distance somewhat greater than 1 cm. To ensure that the screen is in the farfield region for all driving conditions, we place the screen at 3.5 cm (setup in Fig. 3a) or 4.2 cm (setup in Fig. 4a) from the VCSEL. When the CCD-camera is imaging the screen, we place the camera at a distance of 9.7 cm from the screen. If we want to measure in the farfield of the screen, we place the camera at a distance larger than 1 m from the screen. In Figs. 1 and 3a we place a pupil in front of the CCD-camera to enlarge the speckle size in order to ensure that one speckle spot covers at least ten pixels on the CCD chip. The opening diameter of the pupil is approximately 1.5 mm. In Figs. 1–4b we show the measured speckle contrast corresponding to the setups given in Figs. 1–4a.

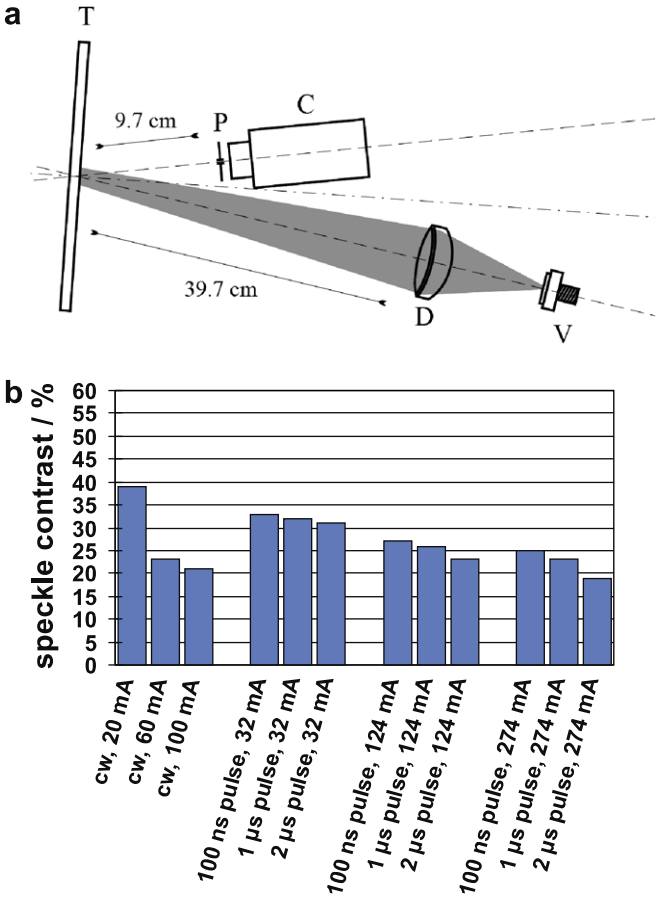

Fig. 1. (a) Projection with a lens (D) of the VCSEL's (V) nearfield onto the screen (T), CCD-camera (C) imaging the paper screen, (b) measured speckle contrasts.

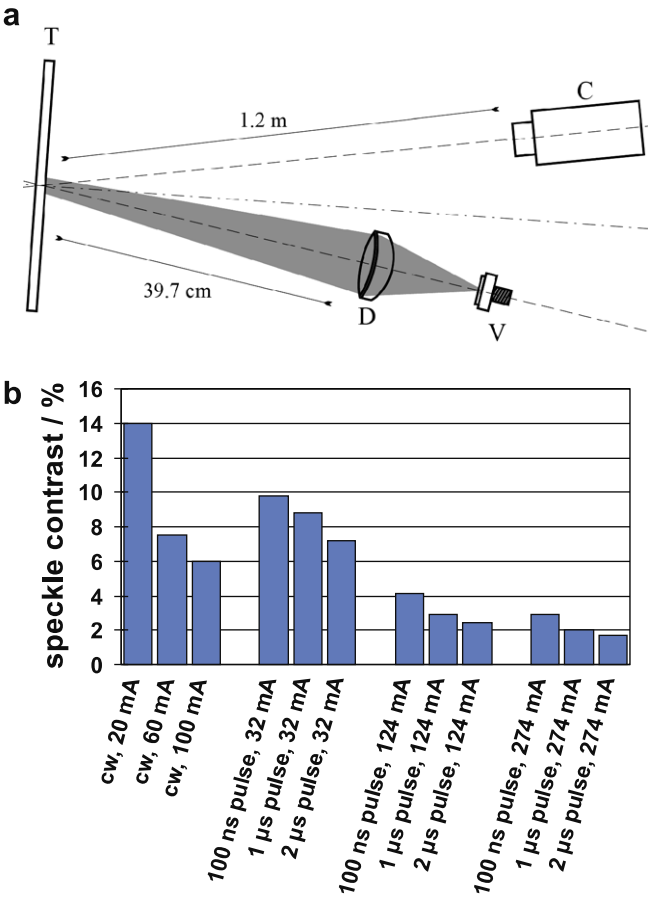

Fig. 2. (a) Projection with a lens (D) of the VCSEL's (V) nearfield onto the screen (T), CCD-camera (C) placed in the farfield of the paper screen, (b) measured speckle contrasts.

3.3. General observations

If we compare Fig. 1b with Fig. 3b and Fig. 2b with Fig. 4b, we observe that the speckle contrast is almost the same whether we project the nearfield or the farfield of the VCSEL on the screen. The speckle contrast is much more dependent on the camera's placement. We clearly measure a much lower speckle contrast when the camera is in the farfield of the screen as compared to the setups when the camera is imaging the screen.

In all four setups, the speckle contrast is decreasing with increasing cw driving current. The lowest speckle contrast in cw operation is achieved in the setup given in Fig. 2a, where the VCSEL's nearfield is projected onto the screen and the CCD-camera is placed in the screen's farfield. The resulting speckle contrast is approximately 6% for a 100 mA driving current.

In pulsed operation, a further substantial speckle contrast reduction can be achieved compared to cw operation. The

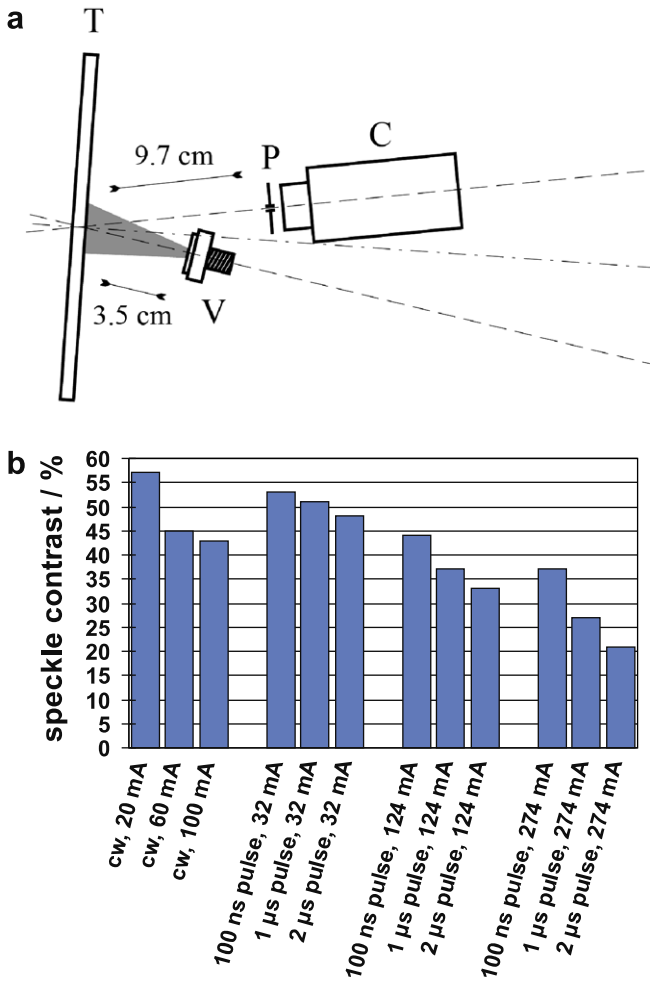

Fig. 3. (a) Projection of VCSEL's (V) farfield onto the screen (T), CCD-camera (C) imaging the paper screen, (b) measured speckle contrasts.

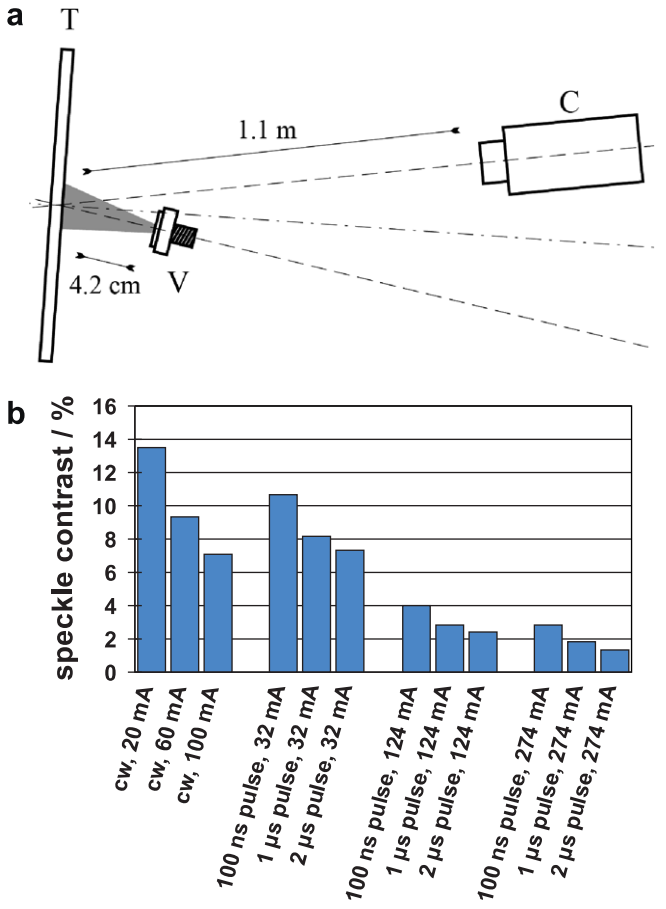

Fig. 4. (a) Projection of VCSEL's (V) farfield onto the screen (T), CCD-camera (C) placed in the farfield of the paper screen, (b) measured speckle contrasts.

speckle contrast decreases with increasing pulse amplitude and length in all investigated setups. The relative decrease with increasing pulse amplitude is significantly more pronounced when the camera is placed in the farfield of the screen (see Figs. 2 and 4). In that case we obtain a speckle contrast as low as 1.7% in Fig. 2 and 1.3% in Fig. 4. If the camera is imaging the screen, the measured speckle contrast is much higher and we do not get the contrast below 19% in case of Fig. 1 and 21% in case of Fig. 3.

4. Estimation of speckle contrast

To interpret our measured contrast values, we describe and estimate the different effects that may contribute to the reduction of the speckle contrast. If several of these effects play a role at the same time, the speckle contrast is obtained by multiplying the individual contrast reduction factors.

4.1. Polarization scrambling paper screen

Paper is known to act as a polarization scrambling screen. For full depolarization, two mutually uncorrelated and orthogonally polarized speckle images are produced, even in case of illumination with a polarized laser. This corresponds to a maximum speckle contrast reduction by a factor of $1/\sqrt{2}$. We already showed in Section 2 that we have full depolarization with the used paper screen.

4.2. Shift of emission wavelength during a pulse

In [14] it is shown that the emission wavelength of the VCSEL in pulsed operation can shift several nanometers. This shift depends on the pulse duration and amplitude and leads to a dynamically changing speckle pattern during the pulse. If the camera integration time is longer than the pulse duration, this results in a reduced speckle contrast. In our measurements the maximum pulse duration is 2 µs, which is much smaller than the camera integration time (the lowest integration time used was 90 µs). Therefore we obtain the same effect as illuminating the screen with a broadband source. The resulting decrease of the speckle contrast is dependent on source and screen parameters. Following [3], the speckle contrast C for broadband illumination of a scattering target is given by

$$C = \sqrt{\int_{-\infty}^{\infty} K_{\hat{G}}(\Delta\nu) \cdot |M_l(\Delta q_z)|^2 \mathrm{d}\Delta\nu}, \tag{1}$$

where $K_{\hat{G}}(\Delta\nu)$ is the autocorrelation function of the source's normalized power spectrum and $M_l(\Delta q_z)$ is the characteristic function corresponding to the path length probability density function $p(l)$ of the photons in a volume scattering screen. Eq. (1) models a fully spatially coherent source. Lateral diffusion effects, the possible overlap of different beamlets and effects of the imaging conditions will not be modeled. With these assumptions, we can simplify Eq. (1) for our volume scattering screen. If we assume that the source has a Gaussian shaped spectrum with a $1/e$ frequency bandwidth $\delta\nu$ which is much smaller than the central frequency $\bar{\nu}$ (central wavelength $\bar{\lambda}$) and if we assume that $p(l)$ has a Gaussian shape with

a standard deviation σ_l, the speckle contrast C under normal illumination and observation can be written as

$$C = \left[1 + 2\pi^2 \cdot (n-1)^2 \cdot \left(\frac{\delta\nu}{\bar{\nu}}\right)^2 \cdot \left(\frac{\sigma_l}{\bar{\lambda}}\right)^2\right]^{-\frac{1}{4}}, \quad (2)$$

where n is the refractive index of paper (cellulose) which is approximately given by 1.5. The assumption of having a Gaussian shaped path length probability density function is reasonable for paper (see for example [15]). Furthermore, small discrepancies from a Gaussian distribution do not result in drastic changes in the speckle contrast [16].

Before we can apply Eq. (2), we need to estimate the standard deviation σ_l, which describes the width of the paper screen's path length probability density function $p(l)$ at the VCSEL's wavelength of 850 nm. We do this via a calibration measurement. We illuminate the paper screen under normal incidence with a pulsed titanium:sapphire (Ti:Sa) laser. This laser has a $1/e$-bandwidth of 5.31 nm when emitting 150 fs pulses and 0.42 nm when emitting 1 ps pulses. The Ti:Sa laser's emission is in the fundamental TEM_{00} mode with a central wavelength of 800 nm. The speckle contrast measured in the screen's farfield (and in the direction normal to the screen) is 20.8 % when 150 fs pulses are used and 57.4% when 1 ps pulses are used. This knowledge of the speckle contrast and the $1/e$ bandwidth of the Ti:Sa laser allows us to use Eq. (2) to calculate the standard deviation σ_l of the function $p(l)$ for the used paper screen. We calculated it to be 2.35 mm at a wavelength of 800 nm. After inserting an external second harmonic generation crystal into the Ti:Sa beam, we analogously determined σ_l to be 4.26 mm for frequency doubled (400 nm wavelength) photons. If we assume the standard deviation of σ_l to decay linearly with increasing wavelength, we can extrapolate σ_l to be 2.12 mm at the VCSEL's wavelength of 850 nm.

To complete the characterization of our VCSEL source, we estimate the heat induced shift in the VCSEL's emission wavelength during a pulse by calibrating the wavelength shift with temperature and by calculating the temperature rise during a pulse [17]. The estimated wavelength shift for the investigated driving pulses can be found in the second column of Table 2. We use these values of the emission wavelength shift as the $1/e$ bandwidth $\delta\nu$ in Eq. (2). In addition, we assume a Gaussian shaped autocorrelation function of the VCSEL's normalized power spectrum $K_{\hat{G}}(\Delta\nu)$. The assumption of $\delta\nu$ being much smaller than the medium emission frequency $\bar{\nu}$ is fulfilled.

The estimated reduction of the speckle contrast because of the shift in the VCSEL's emission wavelength for the used paper screen is shown in the third column of Table 2.

4.3. Reduced spatial coherence

In cw operation a multitude of transverse modes contribute to the emission of the VCSEL. In modal operation, each transverse mode in the cavity is individually fully spatially coherent (if there is no frequency degeneracy of the modes), but the degree of coherence of the superposition of all transverse modes in the cavity is reduced. This behaviour is described theoretically in [18] and measured in [19]. The exact number of modes and the coherence function of the emission are difficult to estimate. Therefore it is difficult to estimate the exact speckle contrast value. Typically, the number of transverse modes contributing to the emission increases with increasing driving current (until the thermal roll-over point is reached). Thus the total beam's spatial coherence and the speckle contrast will decrease with increasing driving current.

In the nonmodal emission regime, the source's aperture is assumed to be filled with independent coherence islands. The size of these islands, relative to the total beam's size, will be different in the VCSEL's nearfield and farfield. In the nearfield, the coherence radius is 1.4 μm whereas the VCSEL aperture radius is 25 μm. The number of independent coherence islands can be estimated by dividing the total VCSEL aperture area by the coherence area. This results in 318 different islands. When we image the VCSEL's nearfield onto the screen, both the VCSEL aperture and the coherence radius will be imaged with the same magnification. Therefore, the number of coherence islands stays the same as in the nearfield of the VCSEL. If we assume that all coherence islands have the same intensity and that they produce speckle patterns which are mutually fully uncorrelated, this results in a maximum speckle contrast reduction by a factor of $1/\sqrt{318} = 0.056$.

For nonmodal emission in the VCSEL's farfield, the situation is slightly different. In that case we can define a coherence radius based on the farfield angular coherence. The farfield coherence angle can be calculated starting from the nearfield intensity distribution [12] and is approximately 1.2° at full-width. This has been confirmed by direct measurements of the farfield coherence angle [12]. After a propagation distance Z, the total beam's radius is equal to $Z\tan(\theta_{1/2})$ where $\theta_{1/2}$ is the half-width divergence angle. Equivalently, the coherence radius is given by $Z\tan(\Phi_{1/2})$ where $\Phi_{1/2}$ is the half-width coherence angle. The number of coherence islands is then given by the ratio of the total beam's area and the coherence area, which yields 344 coherence islands in the farfield of the VCSEL. The maximum speckle contrast reduction is thus $1/\sqrt{344} = 0.054$ if we assume that all coherence islands have the same intensity and produce uncorrelated speckle patterns.

Table 2
Shift in emission wavelength of the VCSEL induced by Joule heating for different pulses

Pulse parameters	Estimated shift in emission wavelength/nm	Estimated speckle contrast reduction factor
100 ns, 32 mA	0.008	0.9993
1000 ns, 32 mA	0.048	0.9796
2000 ns, 32 mA	0.096	0.8212
100 ns, 124 mA	0.045	0.9769
1000 ns, 124 mA	0.270	0.7029
2000 ns, 124 mA	0.540	0.3875
100 ns, 274 mA	0.168	0.9208
1000 ns, 274 mA	1.010	0.5228
2000 ns, 274 mA	2.018	0.2753

Furthermore, the estimated speckle contrast reduction factor is given taking into account quasi-broadband illumination of the volume scattering paper screen.

5. Interpretation of results

5.1. General considerations

The theoretically expected decrease of the speckle contrast with increasing cw driving current is observed for each setup. In pulsed operation, we observe a decrease of the speckle contrast with increasing pulse duration and amplitude because of the increasing thermally induced shift of the VCSEL's emission wavelength. In all four setups, the speckle contrasts measured for a pulse amplitude of 32 mA are significantly higher than those for stronger pulses. This is because the induced thermal dynamics are not strong enough to induce nonmodal emission when the pulse amplitude is only 32 mA. Therefore, the behaviour for a 32 mA pulse is similar to the transverse multimode emission in cw operation with in addition a small thermally induced shift in the emission wavelength. The relative decrease in the measured speckle contrasts for the three investigated pulse lengths fits well with the estimated decrease resulting from the shift in emission wavelength. In the case of a 32 mA pulse of 100 ns pulse length, the influence of the wavelength shift on the speckle contrast is very small (expected

decrease by a factor 0.9997). Therefore, the measured speckle contrast should be between the contrast values for cw operation with 20 mA and 60 mA driving current. This is fulfilled for each setup.

The uncertainty in determining the speckle contrast in modal emission is relatively high (a few percent absolute) because of the non-homogeneously distributed intensity in the captured images, which itself is a result of the modal structure. The extraction of the speckle contrast is much more precise in the nonmodal emission regime. No modal structures are visible and the captured images are much more homogeneously illuminated on a large scale (not the small scale speckle intensity fluctuations).

In the next two sections we scrutinize the speckle characteristics under driving conditions where the VCSEL emits in the nonmodal regime. We restrict this analysis to pulse lengths of 1000 ns and 2000 ns, because the nonmodal emission regime is not yet fully reached after 100 ns.

5.2. Nonmodal emission – projection of VCSEL's nearfield

In case we image the VCSEL's nearfield onto the screen, a large number of coherence islands or beamlets is projected as indicated in Fig. 5. Each beamlet illuminates a region on the screen that is uncorrelated from the regions illuminated by other beamlets. Therefore each beamlet locally produces a speckle pattern that is not correlated with the speckle patterns produced by the other beamlets.

If we image the screen on the CCD chip (setup described in Fig. 1a), we measure many local speckle patterns of high contrast. Each incident beamlet has an approximate diameter of 106 μm on the screen which is sufficiently large to be resolved with the CCD-camera. We therefore only expect two speckle reducing effects to play a role: polarization scrambling (which results in a contrast reduction by $1/\sqrt{2}$) and the shift in the emission wavelength (given in Table 2). A comparison of the measured and the calculated speckle contrast values is given in Table 3.

The measured speckle contrasts are significantly smaller than the estimated values, which is surprising at a first glance. The additional speckle contrast reduction can be explained by taking into account the scattering characteristics of the volume scattering paper screen. The VCSEL's nearfield imaged on the screen looks like the schematic given in Fig. 5a. The photons enter the screen material and are then diffusely scattered. Therefore the backscattered nearfield looks like the schematic given in Fig. 5b. Light from the backscattered beamlets can overlap. The influence of this *lateral* scattering effect is not taken into account when applying Eq. (2). Although photons of different beamlets can leave the screen at the same position, they did a somewhat different random walk, since they entered the screen at different positions. This can result in a speckle contrast reduction in the region of overlap because partially uncorrelated speckle patterns are superimposed in that region.

With these considerations it is reasonable to measure a smaller speckle contrast than expected from our estimates. It is difficult to determine the exact size of the overlapping regions and the mutual correlation of the superimposed speckle patterns. Therefore it is not possible to estimate the absolute speckle contrast values here.

Table 3
Comparison between the measured and estimated speckle contrast for the setup in Fig. 1a

Pulse parameters	Measured speckle contrast/%	Estimated speckle contrast/%
1 μs pulse, 124 mA	26	49.7
2 μs pulse, 124 mA	23	37.0
1 μs pulse, 274 mA	23	27.4
2 μs pulse, 274 mA	19	19.5

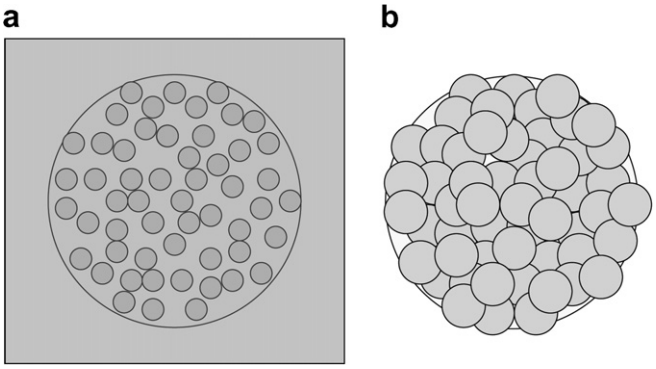

Fig. 5. Schematics of (a) the VCSEL's nearfield incident onto the screen for the nonmodal emission regime. The nearfield consists of about 318 coherence islands. The grey area corresponds to the field of view of the CCD-camera, (b) the VCSEL's nearfield backscattered from the volume scattering screen.

What we can check is the relative decrease of the measured speckle contrast with increasing pulse length and height, as is given in Table 2. The relative decrease corresponds reasonably well with our estimates. Further discrepancies might be related to the assumptions made to derive Eq. (2) in Section 4.2 (Gaussian shaped power spectrum of the VCSEL, model for the thermally induced shift of the VCSEL's emission wavelength and Gaussian shaped path length probability density function of the photons).

If we now move the CCD-camera away from the screen (setup described in Fig. 2a) the interpretation of the measurements becomes simpler. We do no longer image the plane of the screen onto the CCD chip but a plane parallel to the screen at a distance of approximately 1.1 m. Therefore we measure the superposition of all mutually uncorrelated speckle patterns, each of which is produced by a single beamlet. The lateral scattering effects of the screen are now not influencing the measured farfield contrast values. The speckle contrast is thus further decreased by a factor $1/\sqrt{318}$ compared to the estimation given in Table 3. In Table 4 we present a comparison between the measured and the estimated speckle contrast.

There is a good agreement in Table 4 between measurements and estimates in most cases. We measured a minimal contrast of 1.7% which is only slightly higher than the estimated value of 1.3%. This discrepancy might arise from the fact that not all beamlets contribute with the same intensity.

5.3. Nonmodal emission – projection of VCSEL's farfield

The VCSEL's farfield in the nonmodal emission regime is made up of different coherence islands, the size of which is determined by the farfield coherence angle and the propagation distance to the screen. Analogously as in the previous section, the screen is illuminated by coherence islands or beamlets and each beamlet locally produces a speckle pattern that is uncorrelated from the speckle patterns produced by the other beamlets. The difference with the previous section is the size of the total beam and of each beamlet on the screen. For the setups shown in Figs. 3 and 4a, the diameter on the screen of the total beam is 13 mm and 16 mm, respectively and the coherence radius is 0.37 mm and 0.44 mm, respectively.

In case the CCD-camera is imaging the screen (as in the setup shown in Fig. 3a), each coherence island is large enough to be resolved by the camera. Therefore, the number of beamlets on the screen will not influence the speckle contrast and only two speckle reducing effects play a role: polarization scrambling and the shift in the emission wavelength. The speckle contrast estimated based on these two effects is given in Table 5 together with the measured

Table 4
Comparison between the measured and estimated speckle contrast for the setup in Fig. 2a

Pulse parameters	Measured speckle contrast/%	Estimated speckle contrast/%
1 μs pulse, 124 mA	2.9	2.8
2 μs pulse, 124 mA	2.4	2.1
1 μs pulse, 274 mA	2.0	1.5
2 μs pulse, 274 mA	1.7	1.1

Table 5
Comparison between the measured and estimated speckle contrast for the setup in Fig. 3a

Pulse parameters	Measured speckle contrast/%	Estimated speckle contrast/%
1 μs pulse, 124 mA	37	49.7
2 μs pulse, 124 mA	33	37.0
1 μs pulse, 274 mA	27	27.4
2 μs pulse, 274 mA	21	19.5

Table 6
Comparison between the measured and estimated speckle contrast for the setup in Fig. 4a

Pulse parameters	Measured speckle contrast/%	Estimated speckle contrast/%
1 μs pulse, 124 mA	2.8	2.7
2 μs pulse, 124 mA	2.4	2.0
1 μs pulse, 274 mA	1.8	1.5
2 μs pulse, 274 mA	1.3	1.1

speckle contrast values from Fig. 3b. The measured values are smaller than estimated. The additional effect reducing the speckle contrast might again be lateral scattering of the photons, similar to what was suggested when the VCSEL's nearfield is projected on the screen (see Section 5.2). For the investigated setups, the coherence area in the VCSEL's farfield is larger than the coherence area in the projected VCSEL's nearfield. On the other hand, we do not expect the lateral scattering length of the screen to depend on the beam size. Therefore, we expect the additional contrast reduction because of lateral scattering to be smaller in the case where we projected the VCSEL's farfield on the screen compared to the case where we projected the VCSEL's nearfield on the screen. This is confirmed by our experiments: the measured speckle contrasts in Table 5 are clearly higher than those in Table 3. Estimation of the absolute contrast value is again difficult, since the scattering dynamics are not known in detail. As in Section 5.2, we can compare the relative decrease of the measured speckle contrast for the different pulse parameters given in Table 2. The relative decrease fits well with our estimation.

If we place the camera in the farfield of the screen (setup shown in Fig. 4a), we measure the superposition of all the uncorrelated speckle patterns produced by the different coherence islands on the screen. Therefore we expect all three contrast reducing effects discussed in Section 4 to be present: polarization scrambling, shift in the emission wavelength of the VCSEL and the superposition of 334 uncorrelated speckle patterns. A comparison of the measured and the estimated speckle contrast values is given in Table 6. We find a good agreement between measured and estimated contrast values with only small deviations. We obtain a minimal contrast of 1.3%.

6. Conclusion

We investigated the speckle characteristics of a near-infrared broad-area vertical-cavity surface-emitting laser which emits at a wavelength of approximately 850 nm. We compared the speckle characteristics in the multimode and in the spatially incoherent emission regime.

The incoherent emission can help to reduce the speckle contrast, but its full potential to do so was only obtained when the camera is not imaging the screen. In that case we achieved speckle contrast values as low as 1.3%. This is in good agreement with our theoretical estimates of the speckle contrast, where we take into account three speckle contrast reducing effects. These are polarization scrambling of the paper screen, thermally induced shift in the VCSEL's emission wavelength and reduced spatial coherence of the source. This setup is promising for applications which do not image the laser illuminated target and that suffer from speckle noise. An example of such an application is Doppler vibrometry [4].

Ofcourse, for many applications it is required that the screen is imaged onto the detector. When we imaged the screen with full camera resolution onto the CCD chip the lowest measured speckle contrast was 19% in the incoherent emission regime, which is too high for many applications. The reason for this albeit limited speckle contrast reduction is that the beamlets illuminate spatially separated regions on the screen together with the fact that these regions can be resolved by the imaging system. Therefore, we did not get much profit from the spatially incoherent emission of the VCSEL.

One might however unlock the large potential of the incoherent emission regime to reduce the speckle contrast. Two approaches can be considered to achieve this goal. First, if the imaging system is not able to resolve the individual beamlets on the screen, the contrast reduction factor will be proportional to the number of beamlets that fall within the resolution spot of the imaging system. This condition can for example be reached by reducing the size of the VCSEL's beam on the screen. This approach can e.g. be used in laser active triangulation applications [5]. Second, if the different beamlets can be made to overlap, we expect a contrast reduction proportional to the number of beamlets that are overlapping with each other. This can be achieved by using a lens integrator. Such a lens integrator is commonly used in projection applications in order to shape and homogenise the illumination beam. The light passing through different lenses of the lens integrator is illuminating the same area on the screen, but is doing so under slightly different angles. Assuming each of our uncorrelated VCSEL beamlets falls on a different lens of the lens integrator, this would result in many speckle patterns which are (at least partly) decorrelated because of the different illumination angles. Therefore the detectable image will show a reduced speckle contrast. The implementation and testing of these approaches is however beyond the scope of this paper. Nonetheless, this work has provided insight into how and how far the spatially incoherent emission of a VCSEL can be exploited to reduce speckle in various applications.

Acknowledgements

F.R. gratefully acknowledges financial support of the Karlsruhe School of Optics & Photonics (KSOP) and from the European Technology Center (EuTEC) of Sony Deutschland GmbH. G.V., M.P. and I.F. acknowledge financial support of the IAP P6/10 network "Photonics@be" and the VUB-IOF project "Micro-photonics". The authors are indebted to M. Grabherr of U-L-M Photonics GmbH for providing the excellent devices and to G. Craggs for proofreading the manuscript.

References

[1] J.D. Rigden, E.I. Gordon, Proc. IRE 50 (1962) 2367.
[2] B.M. Oliver, Proc. IEEE 51 (1963) 220.
[3] J. Goodman, Speckle Phenomena in Optics: Theory and Applications, Roberts & Company, Englewood, Colorado, 2007.
[4] M. Denman, N. Halliwell, S. Rothberg, Proc. SPIE 2868 (1996) 12.

[5] R.G. Dorsch, G. Häusler, J. Herrmann, Appl. Opt. 33 (7) (1994) 1306.
[6] F. Schieber, SAE Trans. 101 (6) (1992) 797.
[7] P.G.J. Barten, Proc. SPIE 1666 (1992) 57.
[8] C.R. Cavonius, O. Estivez, J. Physiol. 248 (1975) 649.
[9] D.H. Kelly, J. Opt. Soc. Am. 64 (7) (1974) 983.
[10] J.G. Robson, J. Opt. Soc. Am. 56 (1966) 1141.
[11] L. Wang, T. Tschudi, T. Halldórsson, P.R. Pétursson, Appl. Opt. 37 (1998) 1770.
[12] M. Peeters, G. Verschaffelt, H. Thienpont, S.K. Mandre, I. Fischer, M. Grabherr, Opt. Express 13 (2005) 9337.
[13] F. Gori, Opt. Lett. 30 (2005) 2840.
[14] S.K. Mandre, W. Elsässer, I. Fischer, M. Peeters, G. Verschaffelt, Appl. Phys. Lett. 89 (2006) 151106.
[15] C.A. Thompson, K.J. Webb, A.M. Weiner, J. Opt. Soc. Am. A14 (9) (1997) 2269.
[16] F. Riechert, G. Bastian, U. Lemmer, Proc. SPIE 6617 (2007) 661709.
[17] H. Li, K. Iga, Vertical-Cavity Surface-Emitting Laser Devices, Springer, 2003.
[18] E. Wolf, G.S. Agarwal, J. Opt. Soc. Am. A 1 (5) (1984) 541.
[19] M. Bertolotti, B. Daino, F. Gori, D. Sette, Nuovo Cimento 38 (1965) 1505.